

Numerical Simulations of Equatorially-Asymmetric Magnetized Supernovae: Formation of Magnetars and Their Kicks

Hidetomo Sawai¹, Kei Kotake^{2,3} and Shoichi Yamada^{1,4}

hsawai@heap.phys.waseda.ac.jp

ABSTRACT

A series of numerical simulations on magnetorotational core-collapse supernovae are carried out. Dipole-like configurations which are offset northward are assumed for the initially strong magnetic fields together with rapid differential rotations. Aims of our study are to investigate effects of the offset magnetic field on magnetar kicks and on supernova dynamics. Note that we study a regime where the proto-neutron star formed after collapse has a large magnetic field strength approaching that of a “magnetar”, a highly magnetized slowly rotating neutron star. As a result, equatorially-asymmetric explosions occur with a formation of the bipolar jets. We find that the jets are fast and light in the north and a slow and heavy in the south for in rapid cases while they are fast and heavy in the north and slow and light in the south for slow rotation case. Resultant magnetar’s kick velocities are $\sim 300 - 1000 \text{ km s}^{-1}$. We find that the acceleration is mainly due to the magnetic pressure while the somewhat weaker magnetic tension works toward the opposite direction, which is due to stronger magnetic field in the northern hemisphere. Noted that observations of magnetar’s proper motions are very scarce, our results supply a prediction for future observations. Namely, magnetars possibly have large kick velocities, several hundred km s^{-1} , as ordinary neutron stars do, and in an extreme case they could have those up to 1000 km s^{-1} . In each model, the formed proto-magnetar is slow rotator with rotational period of more than 10 ms. It is also found that, in rapid rotation models, the final configuration of the magnetic field in the proto-magnetar is a

¹*Science & Engineering, Waseda University, 3-4-1 Okubo, Shinjuku, Tokyo 169-8555, Japan*

²*Division of Theoretical Astronomy, National Astronomical Observatory of Japan, 2-21-1 Osawa, Mitaka, Tokyo 181-8588, Japan*

³*Max-Planck-Institute für Astrophysik, Karl-Schwarzschild-Str. 1, D-85741, Garching, Germany*

⁴*Advanced Research Institute for Science & Engineering, Waseda University, 3-4-1 Okubo, Shinjuku, Tokyo 169-8555, Japan*

collimated dipole-like field pinched by the torus of toroidal field lines whereas the proto-magnetar produced in the slow rotation model is totally poloidal-field dominant.

Subject headings: supernovae: general — supernovae: general — pulsars: general — stars: magnetic fields — MHD — methods: numerical

1. Introduction

Soft-gamma repeaters (SGRs) and anomalous X-ray pulsars (AXPs) are candidates of so-called “magnetars”, highly magnetized slowly rotating neutron stars. This is based on the “magnetar model”, i.e. their burst-like activities, persistent X-ray emissions, and large spin-down rates will originate from high magnetic fields, $B \gtrsim 10^{14} - 10^{15}$ G (Duncan & Thompson 1992; Paczyński 1992; Thompson & Duncan 1995, 1996). It is notable that such a large magnetic field also may power supernova explosions (magnetorotational supernova). Thus, study of magnetorotational supernovae may be important in the context of magnetar formations.

The first paper concerning magnetorotational supernovae written by LeBlanc & Wilson (1970) appeared about 30 years before the idea of “magnetar model” has arisen. They found that strong magnetic field combined with rotation produced an asymmetric supernova explosion. Only a few studies followed after this (Bisnovatyi-Kogan et al. 1975; Müller & Hillebrandt 1979; Ohnishi 1983; Symbalisty 1984), reflecting a feeling that magnetic fields large enough to drive supernovae were thought to be unrealistic. Now that such high magnetic fields are observationally supported, the magnetorotational supernova is attracting more attention than before. In the last several years some papers have been published on the magnetorotational supernovae (e.g. Wheeler et al. 2002; Akiyama et al. 2003; Yamada & Sawai 2004; Kotake et al. 2004; Takiwaki et al. 2004; Ardeljan et al. 2005; Kotake et al. 2005; Sawai et al. 2005; Obergaulinger et al. 2006; Nishimura et al. 2006; Moiseenko et al. 2006; Shibata et al. 2006). Although, with these studies we have developed our understanding of magnetorotational supernovae, many issues still remain to be investigated. For example, neutron star’s kicks in the context of magnetorotational supernovae (magnetar’s kicks) have not been studied fully numerically. (see, however, Kotake et al. (2005): they computed the parity-violating effects in strongly magnetized supernova cores and expected that neutron star’s kicks would result.) In fact, all numerical simulations of magnetorotational core-collapse so far assumed equatorial symmetry and computed only a quarter of a meridional plane of the star.

Observed neutron stars are known to have generally larger proper velocities than that of their progenitor stars (Gunn & Ostriker 1979). Their three-dimensional velocities are

typically several hundred km s^{-1} and some of them have a speed higher than 1000 km s^{-1} (e.g. Cordes & Chernoff 1998; Hobbs et al. 2005). The origin of the proper velocities is still controversial. Although many researchers agree that an asymmetric supernova explosion is a more promising origin rather than a binary-system disruption by a supernova explosion, several different mechanisms have been proposed, which can be categorized mainly into three classes (Lai 2003).

The first mechanism is a hydrodynamically-driven kick. Scheck et al. (2006) numerically studied hydrodynamic instabilities in neutrino-driven supernova explosions and showed that neutron stars were accelerated up to about $500 - 1000 \text{ km s}^{-1}$ due to the dominance of $l = 1$ mode. In their numerical simulations neutron stars are substituted with gravitating inner boundaries. Fryer & Warren (2004) performed three-dimensional SPH simulations and asserted that neutrino asymmetries decelerated a kicked neutron star significantly, which Scheck et al. (2006) argued were negligible. The second mechanism is a neutrino-magnetic-field driven kick. Lai & Qian (1998) studied a possibility that an asymmetric field topology could produce a large kick when combined with neutrino emission. They pointed out problems in former similar works and improved on how to deal with microphysics. The conclusion which they derived was that at least $\sim 10^{16} \text{ G}$ difference of magnetic field strength between the north and south poles of a proto-neutron star is necessary to get 300 km s^{-1} kick velocity. Arras & Lai (1999) investigated parity violation effects on neutron star’s kick with again improved microphysics. They argued that for the generation of the kick velocity of a few hundred km s^{-1} , at least $10^{15} - 10^{16} \text{ G}$ of dipole magnetic field is necessary in a proto-neutron star. The third mechanism is an electromagnetically-driven kick, which was suggested by Harrison & Tademaru (1975). According to their analysis neutron star’s kick velocity of several hundreds km s^{-1} can be generated when the initial rotation period of pulsar is $\sim 1 \text{ ms}$ though with the initial rotation period of $\sim 10 \text{ ms}$ the result will be two orders of magnitude smaller than the former velocity. This mechanism does not depend on the strength of magnetic fields. The main difference from the other two mechanisms is a time scale of kick generation. With a surface field of $\sim 10^{12} \text{ G}$ and an initial rotation period of $\sim 1 \text{ ms}$, the acceleration time scale of a pulsar is approximately five years.

In this paper we consider an another class mechanism, “*magnetohydrodynamically-driven kick*”. Consider the situation that the rapidly rotating core has the dipole-like magnetic field which is somewhat offset from the center of the core prior to collapse. Then, it is expected that a supernova with equatorially-asymmetric bipolar jet will occur. This will lead to a kick of the neutron star. Magnetar-class strong magnetic field is required for this mechanism to work. If this were to a kick mechanism of ordinary neutron stars, the magnetic field must decay from $\sim 10^{15} - 10^{16} \text{ G}$ to $\sim 10^{12} \text{ G}$. (This is also the case for the second mechanism above.) Goldreich & Reisenegger (1992) estimated the decay time scales of the magnetic field

in a neutron star due to Ohmic dissipation or ambipolar diffusion. Their results imply that the magnetar-class magnetic fields confined in neutron stars require at least $\sim 10^6 - 3 \times 10^7$ years to decay to the strength of typical neutron stars ($\sim 10^{12}$ G). This is much longer than the ages of not small number of ordinary pulsars. Hence, we ignore the kicks of ordinary pulsars here, but are concerned only with the kicks of magnetars.

According to the “*magnetohydrodynamically-driven kick*” mechanism, we numerically study the core-collapse of massive star with off-centered strong dipole-like magnetic fields and rapid rotation.

The initial magnetic field strength chosen here corresponds to the magnetar-class or larger ($\sim 10^{15} - 10^{16}$ G) when the core contracts to a typical neutron-star radius. This means that we adopt a so-called fossil origin hypothesis of magnetic fields in magnetars. Although the origin of magnetic fields in magnetars are still a mystery, Ferrario & Wickramasinghe (2005) asserted that the magnetic flux of θ Orionis C, which is an O star, corresponds to that of magnetars and that the magnetism of magnetars could be explained as the fossil of progenitors as in the case of white dwarfs (Wickramasinghe & Ferrario 2005). In fact, the magnetic flux of θ Orionis C is $\sim 1 \times 10^{27}$ G cm², which corresponds to $\sim 10^{15}$ G of the surface field if a neutron star is formed with the frozen magnetic field. There are several other OB stars suggested observationally to possess magnetar-class magnetic fluxes. For example, the estimated magnetic flux of HD191612 (Donati et al. 2002) corresponds to the surface field strength of $\sim 5 \times 10^{15}$ G, whereas several $\sim 10^{14}$ G of surface magnetic fields are expected for ζ Cassiopeiae (Neiner et al. 2003a), ω Orionis (Neiner et al. 2003b), ξ CMa (Hubrig et al. 2006) and V2052 Ophiuchi (Neiner et al. 2003c) if their magnetic fields are compressed in the formation of a neutron star. Among them, θ Orionis C and HD191612 are O stars while the others are B stars. On the other hand, Thompson & Duncan (1993) proposed that strong magnetic fields of magnetars originate from the convective dynamo process, which requires a rotation period shorter than ~ 30 ms. However, whether such a process really operates in neutron stars or not, is still uncertain. In this paper, we take a scenario that some OB stars have large magnetic fluxes and end up with a magnetar (fossil origin hypothesis). Although the initial magnetic fields assumed in this study are still a little larger than those implied by above observations, we are exploring the extreme limit.

The offset of the magnetic field in our computation may be supported by numerical simulations of fossil magnetic field in A stars and white dwarfs carried by Braithwaite & Spruit (2004). They found that initially random magnetic fields evolved into a coherent dipole-like field configuration stabilized by a torus of twisted magnetic field lines. This magnetic field diffuse within $\sim 10^9$ years which is much longer than life time of massive stars. We would like to stress that the resultant magnetic field was usually somewhat offset from the center

of the star. Note that they assumed fossil origin hypothesis of magnetic field which we also adopt here.

The rotation period assumed in our rapid rotation models (see § 2) is an order of magnitude shorter than the result of Heger et al. (2005) who calculated the evolution of rotating massive stars. In spite of the importance of their study, it is not still the conclusion. The angular momentum distributions at the pre-collapse stage should be studied further in the future. Our position is that they are not well-known yet and just consider the extreme case.

Since observations of magnetar kick velocities are very scarce so far, our standpoint in this paper is predicting future observations of magnetar’s proper velocities. Proper motions have been measured for only two magnetar candidates (both are AXPs), in which just upper limits were put; $\lesssim 1400(D/10 \text{ kpc}) \text{ km s}^{-1}$ for 4U0142+61 (Hulleman et al. 2000; Woods & Thompson 2006) and $\lesssim 2500(D/3 \text{ kpc}) \text{ km s}^{-1}$ for 1E2259+586 (Ögelman and Tepedelenlioglu 2005). Gaensler et al. (2001) examined the reliability of AXP/SGR association with supernova remnants (SNRs). The associations which they considered probable enable us to estimate velocities of AXPs and SGRs from their positions in the SNRs: $< 500 \text{ km s}^{-1}$ for AXP 1E 1841-045, $< 400 \text{ km s}^{-1}$ for AXP 1E 2259+586, and $< 500 \text{ km s}^{-1}$ for AX J1845-0258 (AXP candidate) (Gaensler et al. 2001, and reference their in). Cline et al. (1982) evaluated the velocity of SGR 0526-66 assuming that it is associated with SNR N49 and derived $v_{kick} \sim 400 - 1400 \text{ km s}^{-1}$. Corbel et al. (1999) derived $\sim 800 - 1400 \text{ km s}^{-1}$ velocity of SGR 1627-41 from the association with SNR G337.0-0.1. However, Gaensler et al. (2001) insisted that these two associations between the SGRs and the SNRs are less convincing.

Recently, we reported the results of numerical study that configurations of magnetic fields affect supernova dynamics significantly (Sawai et al. 2005). The effects of the offset dipole field on the supernova explosion is another subject which we are interested in this paper. We particularly focus on how dynamics and the explosion energy are altered and that north-south difference of the magnetic and rotational energies.

The rest of this paper organized as follows. We describe numerical models such as basic equations, a equation of state, magnetic field and rotation, and the definition for proto-magnetar in § 2. In § 3, the some numerical results including dynamics and kick velocities are shown. In § 4, we give some discussions and conclude the paper.

2. Models

We numerically simulate the core-collapse of magnetized massive stars with the numerical code ZEUS-2D developed by Stone & Norman (1992). A $1.5M_{\odot}$ core of $15M_{\odot}$ star provided by Woosley (1995) is chosen as a pre-collapse model, which gives spherically symmetric profiles of the density and specific internal energy. Magnetic field and rotation are just added to the core by hand (see §2.3).

2.1. Basic Equations

The following ideal MHD equations are solved:

$$\frac{D\rho}{Dt} + \rho\nabla \cdot \mathbf{v} = 0, \quad (1)$$

$$\rho \frac{D\mathbf{v}}{Dt} = -\nabla p - \rho\nabla\Phi + \frac{1}{4\pi}(\nabla \times \mathbf{B}) \times \mathbf{B}, \quad (2)$$

$$\rho \frac{D}{Dt} \left(\frac{e}{\rho} \right) = -p\nabla \cdot \mathbf{v}, \quad (3)$$

$$\frac{\partial \mathbf{B}}{\partial t} = \nabla \times (\mathbf{v} \times \mathbf{B}), \quad (4)$$

where ρ , \mathbf{v} , p , e , Φ , \mathbf{B} are the density, velocity, internal energy density, gravitational potential, and magnetic field, respectively. We denote the Lagrangian derivative as $\frac{D}{Dt}$.

A computational region is a half of the meridional plane with axisymmetric assumption. $200(r) \times 60(\theta)$ grid points extending to 2000 km are used initially. After central density reaches $10^{12} \text{ g cm}^{-3}$, we change the radial mesh resolution and a radius of outer boundary into $300(r)$ and 1500 km, respectively. The radial grid spacing are not uniform with a finer resolution for smaller radii, while the angular grid points are put uniformly.

2.2. Equation of State

As in the previous papers by Yamada & Sawai (2004) and Sawai et al. (2005), we use a parametric EOS which was first introduced by Takahara & Sato (1984). Although we drastically simplify complicated microphysics such as the neutrino transport, it is not a serious concern since our computation is done only on the time scale of prompt explosion, during which the neutrino transport is less important.

The parametric EOS we employed in this paper is as follows;

$$p_{tot} = p_c(\rho) + p_t(\rho, e_t), \quad (5)$$

$$p_c(\rho) = K\rho^\Gamma, \quad (6)$$

$$p_t(\rho, e_t) = (\gamma_t - 1)\rho e_t. \quad (7)$$

The pressure consists of two parts, the cold part (p_c) and the thermal part (p_t). The thermal part is a function of the density and the specific thermal energy, e_t , in which γ_t is the parameter called the thermal stiffness. The cold part is a function of the density alone where the two constants, K and Γ , take account of the effect of the degeneracy of leptons and the nuclear force. We choose the same values for γ_t , K and Γ as in Sawai et al. (2005), so that a numerical simulation without either magnetic field or rotation fails to explode as in recent realistic simulations. Readers are referred to the paper by Sawai et al. (2005) for more details about this EOS.

2.3. Magnetic field and Rotation

The initial magnetic field is assumed to have a dipole-like structure produced by the sum of the line currents which are uniformly distributed in the spherical region within a 1500 km radius. The equatorially-asymmetric dipole magnetic field is obtained by displacing equatorially-symmetric field along the rotation axis. Then the initial magnetic field in the cylindrical coordinate is given by

$$B_\varpi(\varpi, z) = \frac{2J}{c} \sum_{\varpi_J} \sum_{z_J} \frac{z'}{\varpi \sqrt{(\varpi_J + \varpi)^2 + z'^2}} \left[-K + \frac{\varpi_J^2 + \varpi^2 + z'^2}{(\varpi_J - \varpi)^2 + z'^2} E \right], \quad (8)$$

$$B_z(\varpi, z) = \frac{2J}{c} \sum_{\varpi_J} \sum_{z_J} \frac{1}{\sqrt{(\varpi_J + \varpi)^2 + z'^2}} \left[K + \frac{\varpi_J^2 - \varpi^2 - z'^2}{(\varpi_J - \varpi)^2 + z'^2} E \right], \quad (9)$$

$$z' = z - z_J - z_{off}, \quad (10)$$

where R is a distance from the center, and (ϖ_J, z_J) is the mesh point where the line currents exist. J , K , E , c , and z_{off} are the current, complete elliptical integral of the first kind, complete elliptical integral of the second kind, the speed of light, and the degree of offset, respectively. We compute with changing the magnetic field strength and degree of offset (see Table 1). Note that, if the result of Braithwaite & Spruit (2004) is adopted to the iron core of a 2000 km radius, the degree of displacement is several hundred km. Fig. 1 shows the initial magnetic field configuration of models MR3 and SR10 (for the name of models, see below).

The initial angular velocity in our simulations is assumed to have a differentially rotating distribution,

$$\Omega(r) = \Omega_0 \frac{r_0^2}{r_0^2 + r^2}, \quad (11)$$

where Ω_0 and R_0 are constants. With this distribution, rotation is faster at small radii. In all models, $R_0 = 1000$ km is chosen, with which the initial differential rotation is rather mild. We compute the models with rapid rotation and slow rotation cases (see Table 1). The rapid and slow rotation correspond to a neutron star rotating with the period of ~ 1 ms and ~ 10 ms, respectively, if the angular momentum conservation is assumed.

In Table 1, six models computed are summarized. The name of each model consists of three parts, two characters and a number. The first character denotes a strength of magnetic field; “Moderate” and “Strong”. The second character represents a rotation period, “Slow” and “Rapid”. The attached number stands for a degree of magnetic-field displacement. For example, model MR3 has a moderate magnetic field, rapid rotation and the displacement of 300 km.

2.4. Definitions of a Proto-Magnetar and its Velocity

We define a proto-magnetar (or a proto-neutron star) in our analysis as a region which has a mass of $1.2M_\odot$. The mass of each fluid element is summed up descending order of the density. This is almost the maximal mass of fluid which remains through the simulations in the numerically active region and does not go out of the outer boundary. Neutron stars in binary systems typically have the mass of around $1.4M_\odot$ (e.g. Taylor & Weisberg 1982; Thorsett & Chakrabarty 1999). However, the mass of magnetar candidates is unknown at present. Scheck et al. (2006) discussed that resultant mass of neutron star decreases as explosion time scale becomes short. If explosion occurs in a prompt manner, a $1.2M_\odot$ magnetar may not be so bad.

The velocity of the proto-magnetar is defined as follows,

$$v_{NS}(t) = \int_{t_0}^t \frac{F(t')}{M_{NS}} dt', \quad (12)$$

$$F(t) = \oint_{S_{NS}} \left(-P\mathbf{n} - \frac{B^2}{8\pi}\mathbf{n} + \frac{B_z}{4\pi}\mathbf{B} \right) \cdot \mathbf{n}_z dS - \int_{V_{NS}} \rho \nabla \Phi_{outer} dV, \quad (13)$$

where, \mathbf{n} , \mathbf{n}_z , and Φ_{outer} represent a local unit vector normal to each surface element on a proto-magnetar, a unit vector parallel to the rotation axis, and the gravitational potential attributed to mass distribution in the outer layer of the proto-magnetar, respectively. t_0 is

the time when the central density reaches $1.0 \times 10^{12} \text{ g cm}^{-3}$, before which the acceleration of the proto-magnetar is negligible.

The velocity of a magnetar also could be defined in principle as the center of mass velocity. However we do not adopt this definition here because it leads to enormous numerical errors in calculating the volume integral of momenta over the region of the proto-magnetar. The velocity at each grid point is obtained by the time-integration of the volume forces (pressure gradient, Lorentz force and gravity) exerted there and the advection term. Hence, the volume integral of the momentum over the proto-magnetar is equal to the time integration of the volume integral of these forces and the advection term over the proto-magnetar. The difficulty in the numerical estimation of the proto-magnetar’s kick velocity lies in the volume integral of the forces and the advection term. In fact, the error in calculating the proto-magnetar’s kick velocity in this way comes not only from the surface of the proto-magnetar but also from its entire volume, and the problem is that the values of the integrand at the center are greater by a few orders of magnitude than those at the surface of the proto-magnetar and, as a result, errors of a few percent around the central region of the proto-magnetar correspond to errors of more than 100 percent around the surface. On the other hand, if we calculate the proto-magnetar’s kick velocity by time-integrating the surface forces, the resultant numerical errors originate from the local errors in the forces on the proto-magnetar surface and their magnitude will be comparable to the typical error, namely a few percent. This corresponds to an error of a few 10 km/s in the proto-magnetar’s kick velocity in model MR3, for example. It should be noted that the employment of a conservative scheme does not guarantee the correct spatial distribution of momentum. Moreover, since the self-gravity cannot be written in a conservative form, the strict conservation of the total momentum cannot be expected after its inclusion.

3. Results

We show the numerical results of our computation in this section. The explosion dynamics, explosion energies, final states of magnetic field and rotation, and magnetar kicks are given separately.

3.1. Dynamics

We first describe the dynamics of each model. The important parameters for all models are summarized in Table 2 and 3.

Model MR0 has the same initial parameters as model C10 of Sawai et al. (2005) except for the magnetic field configuration. The magnetic field of C10 was parallel to the rotation axis and its strength was stronger near the rotation axis while the magnetic field of model MR0 is dipole-like with larger strength near the center. Namely, model MR0 is a more “centrally” concentrated counterpart of model C10. The dynamical evolution of model MR0 is described as follows. Model MR0 first bounces at 142.7 ms after the onset of collapse when the central density reaches $3.75 \times 10^{14} \text{ g cm}^{-3}$. However the first shock wave is generated not by the nuclear force but by the magnetic force 0.2 ms prior to the nuclear bounce around a radius of 30 km near the rotation axis, which was also the case for model C10 in Sawai et al. (2005). Indeed the magnetic field around the region is strong enough by the time of bounce due to the compression and field wrapping that the magnetic pressure becomes much larger than the matter pressure. Then, the magnetic-force-dominant regions gradually spread outward and shock waves propagate through the core accompanied by the formation of a bipolar jet. This occurs by transferring the magnetic energy to the kinetic energy. As shown in left panel of Fig. 2 and its inset, the toroidal energy is produced by the rotational energy especially around the time of the first bounce (~ 143 ms) and the subsequent second bounce (~ 147 ms). After the amplifications, the toroidal magnetic energy clearly decreases as the kinetic energy of matters whose radial velocity is positive (the outward kinetic energy) increases. The toroidal energy is not only consumed to launch the jets but also continues to be produced by the rotational energy during this phase. This is why the rate of the outward kinetic energy increase is larger than that of the toroidal energy decrease. The poloidal field energy also will be transferred into the kinetic energy although the total poloidal magnetic energy itself increases with time as the matter falls. The outer most shock front reaches a radius of 1500 km, 20 ms after the bounce (see top left panel of Fig. 3). The explosion energy at that time is 4.4×10^{51} erg, which is almost twice as large as the most explosive model C10 in Sawai et al. (2005). This implies that centrally concentrated magnetic fields tends to explode supernovae more powerfully.

Offset magnetic field models with rapid rotation, MR3, SR3 and SR10, produce equatorially-asymmetric explosions with the faster jet northward, in which the degree of asymmetry is the most remarkable for model SR10. (see Fig. 3). In these models, shock waves are generated also prior to the nuclear bounce due to the magnetic force, which occurs first in the northern hemisphere and then in the southern hemisphere with $\sim 0.1 - 0.6$ ms delay. Then the shocks propagate through the core with larger speed northward. The magnetic energy is more dominant in the northern hemisphere than in the southern hemisphere almost always until the shock reaches the surface of the core although the toroidal part is larger in the southern hemisphere (Fig. 4). This is why the jet and shock propagation are faster in the north.

We show the reason why the toroidal magnetic energy is larger in the southern hemisphere. The time evolutions of the rotational energies in Fig. 4 show that matter collapses more deeply in the northern hemisphere around the first bounce for models MR3 and SR3¹. This is because the stronger magnetic fields in the northern hemisphere extract the rotational energy more efficiently, which results in that the centrifugal force reduces and the matter falls favorably. On the other hand, the same interpretation is not valid for model SR10, in which the collapse is deeper in the southern hemisphere in turn around the first bounce. It is considered that magnetic field not only encourages the collapse by extracting the rotational energy, but also discourages it. The latter effect occurs simply because the magnetic force preclude the matter from falling where it is dominant, i.e. around the rotation axis with a radius more than ~ 100 km for the rapid rotation models. Note that, for every model computed here, there always locally exist the region where the magnetic pressure dominates the matter pressure during collapse, and so this effect is significant in spite of the fact that the total magnetic energy is much smaller than the rotational energy. This effect seems to work well in model SR10. It is likely that too strong magnetic field is disadvantageous for the infall of the matter. For the second bounce in each model, the magnetic field rather works to decrease the infall rate which leads to deeper collapse in the southern hemisphere since the magnetic field grows larger than that at the first bounce. As a result, the rotational energy becomes larger in the northern hemisphere after the second bounce, and thus the toroidal magnetic energy also becomes larger.

Table 3 shows that the mass ejection in the southern hemisphere is larger than that in the northern hemisphere for model MR3². This is explained by the effect mentioned above, i.e. the magnetic force prevents the matter infall. An amount of ejected mass is determined by how much matter is accumulated around the outside of the boundary between the inner and outer cores when the shock waves are generated. In fact, it is the outer core where the braking of infall by the magnetic forces works. Owing to stronger magnetic field, the mass infall in the outer core is more effectively hampered in the northern hemisphere although the larger gravitational energy is extracted in the northern hemisphere around the first bounce for models MR3 and SR3 and so at least the inner core collapses well in this half. As a result, mass eruption is smaller in the northern hemisphere. According to Yamada & Sato (1994), the amount of available gravitational energy is sensitive to the ejected mass for the prompt explosion with pure rotation. However it will not be said for magnetorotational case.

¹The two bumps in the rotational energy evolution in each panel of Fig. 4 roughly show how deeply the core collapses, reflecting the gravitational energy evolution.

²The ejected mass is defined as the sum of the mass of fluid elements with the positive total energy. With this definition, a part of mass in the proto-magnetar is also summed.

In summary, we find that the jets are right and fast in the northern hemisphere and heavy and slow in the southern hemisphere for the rapid rotation cases.

The slow rotation models, MS3 and SS3, produce an order of magnitude weaker explosions than rapid rotation models. The expelled masses are also smaller by an order of magnitude (see Table 3). In each of the two models, the magnetic field plays a dynamical role only just behind the shock fronts as they expand outward. However, unlike in the rapid rotation cases, the toroidal magnetic field plays almost no role to power the shock but probably the poloidal field single-handedly does. In fact the slow rotation can not yield strong toroidal fields whose energy is enough to help explosion (see Fig. 2). The farthest shock front reaches a radius of 1500 km about 70 ms after the bounce, which is 3.5 times longer than for model MR3. Contrary to the rapid rotation models, the slow rotation models expel more mass in the northern hemisphere (see Table 3). This is because the magnetic pressure during bounce is not strong enough to hamper the collapse (see right panel of Fig. 2) and the magnetic field just acts to extract the rotational energy. Thus for the slow rotation models, the jets are heavy and fast in the northern hemisphere and right and slow in the southern hemisphere.

3.2. The Explosion Energy

The explosion energies for all model is given in Table 3. They are estimated by the sum of the energies over the fluid elements with the positive total energy when the shock front reaches a radius of 1500 km. It can be seen that for the rapid rotation models the offset dipole field weakens the explosion in comparison of MR0 with MR3 and of SR3 with SR10. For model MR3, the explosion energy in the northern hemisphere is somewhat smaller than that of model MR0 while the explosion energy in the southern hemisphere is just slightly larger than that of model MR0, which makes model MR3 weaker exploder. These features are just reflected by the amounts of the ejected mass, i.e. the larger mass ejected, the stronger the explosion becomes (see Table 3). Namely, in this case, the explosion energy is also controlled by the degree of infall in the outer core as the amount of the ejected mass. For the comparison between models SR3 and SR10, the situation is different. Although the expelled mass is larger for model SR10, the explosion energy is larger for model SR3. This is because the stored magnetic energy after the bounce for model SR3 is much larger than that for model SR10 both in the northern and southern hemispheres (see Fig. 4). For model SR10, the magnetic field is very sparse in the southern hemisphere from the beginning. Meanwhile, in the northern hemisphere, in spite of initially very strong magnetic field it can not be amplified so much since the increase of rotational energy due to collapse is very small

(see § 3.1). Not same as the rapid rotation models, the explosion energy is larger in the northern hemisphere for the slow rotation models. This is simply because mass ejection is larger in the north (see § 3.1). After all, what we find here is that the magnetic fields which induce the explosions also work against the energetic explosions.

3.3. Formation of A Proto-Magnetar

The proto-magnetars which we call in this paper were defined in § 2.4. They have much different shapes between the rapid rotation models and slow rotation models. In upper two panels of Fig. 5, the final shape of the proto-magnetars for model MR3 and MS3 can be seen. For model MR3, this corresponds to the region whose density is more than $2.0 \times 10^7 \text{ g cm}^{-3}$ and the proto-magnetar has a butterfly-like shape in the meridional plane, occupying large fraction in the computational domain. On the other hand, the proto-magnetar of model MS3 whose critical density is $7.8 \times 10^9 \text{ g cm}^{-3}$, has only a radius of $\sim 100 \text{ km}$ and its shape is a oblate ellipsoid.

Final rotation-period profiles for models MR3 and MS3 are also displayed in upper two panels of Fig. 5. For model MR3 the constant Ω surface in the proto-magnetar is rather cylindrical than spherical because the matter is expelled strongly toward both poles. There exist a slowly-rotating torus with a $\sim 100 \text{ km}$ radius in the inner region of the proto-magnetar. Starting from the surface of the torus, narrow zones where the angular velocities are also small run along the inner line of the wings of the “butterfly”. In the proto-magnetar, there is almost no region whose rotation period is smaller than 10 ms. In model MS3, the angular momentum distribution is disarray especially at small radii though at large distances from the rotation axis it is marginally cylindrical. All fluid elements rotate with a rotation period of about a few seconds in the proto-magnetar.

The magnetic field distribution at the end of simulations is shown in lower panels of Fig. 5. In model MR3, a region where the poloidal field is strong spindles along the rotation axis to the surface of the core due to the formation of the strong bipolar jet. The poloidal field has a collimated dipole-like shape around the rotation axis and no longer much off-centered as before while the toroidal field is somewhat equatorially-asymmetric. Around the foot of the jets and the inner part of the proto-magnetar, the toroidal fields are very weak since their energy is transferred into the kinetic energy of jets. On the other hand, in the outer part of the proto-magnetar (the wings of the “butterfly”), the toroidal field is dominant in most area. The global magnetic field structure is roughly such that the dipole magnetic field pinched by the toroidal magnetic field lines, the region with more than $\sim 10^{13} \text{ G}$ regarded. How this magnetic fields will evolve during cooling of the proto-magnetar to a

magnetar of ~ 10 km radius is of another interest which should be investigated elsewhere in the future. In model MS3, areas where the toroidal field is comparable to the poloidal field are very small. There is a cylinder at the center of the core with ~ 1400 km length and ~ 400 km radius (a blue-colored cavity in Fig. 5) where is totally poloidal-field dominant. The proto-magnetar is in the most inner part of this cylinder, in which the toroidal field is especially weak. The poloidal field is also non-offset dipole-like but is not as collimated as in the case of model MR3 owing to weakly ejected mass.

3.4. Kick Velocity of a Nascent Magnetar

We show, in Fig. 6, the time evolution of velocities of the proto-magnetars for all models. Models MR3, MS3, SR3 and SS3 produce kick velocities of around $350 - 500$ km s $^{-1}$ while model SR10 yields a velocity of more than 1000 km s $^{-1}$. Note that in the equatorially-symmetric model MR0, the velocity of the proto-magnetar is less than 70 km s $^{-1}$, which are due to un-removable numerical noises. The final velocities are estimated at 240 ms from the beginning of computations.

In model MR3, the proto-magnetar is kicked southward and finally reaches a kick velocity of 512 km s $^{-1}$. As shown in Fig 7, the driving force is the magnetic pressure. Since the magnetic pressure generally pushes the matter and the magnetic energy is superior in the northern hemisphere (see Fig. 4³), the proto-magnetar is pushed southward. Meanwhile, the magnetic tension which generally pulls the matter works northward again with the help of stronger magnetic field in the northern hemisphere although this is somewhat weaker than the magnetic pressure. Now we discuss what determines which of these two stresses becomes dominant. The z-component of the force owing to magnetic pressure and tension of the poloidal field in cylindrical coordinates are

$$F_{mp,z} = -\frac{1}{8\pi} \int_S B^2 dS_z = -\frac{1}{8\pi} \int_S B^2 \cos \theta_2 dS, \quad (14)$$

$$F_{mt,z} = \frac{1}{4\pi} \int_S B_z \mathbf{B} \cdot d\mathbf{S} = \frac{1}{4\pi} \int_S B^2 \cos \theta_1 \cos(\theta_1 - \theta_2) dS, \quad (15)$$

where, $B^2 = B_z^2 + B_R^2$, and θ_1 and θ_2 is the angles of the magnetic field and surface element vector measured from the rotation axis, respectively. We consider here in the range $\theta_2 - 90^\circ \leq \theta_1 \leq \theta_2 + 90^\circ$ and $-90^\circ \leq \theta_2 \leq 90^\circ$, i.e. the magnetic field is outward on the surface in the northern hemisphere. A contribution by the toroidal field is omitted for simplicity for the

³This figure does not shows the magnetic energies just around the proto-magnetar but those integrated over the northern or southern hemisphere. Hence, it gives just a rough indication here.

moment. Where the magnetic tension is locally dominant, the following relation works out from Eqs. (14) and (15),

$$2B^2 \cos \theta_1 \cos(\theta_1 - \theta_2) - B^2 \cos \theta_2 = \cos(2\theta_1 - \theta_2) \geq 0, \quad (16)$$

and then θ_1 satisfies

$$\frac{\theta_2}{2} - 45^\circ \leq \theta_1 \leq \frac{\theta_2}{2} + 45^\circ, \quad (17)$$

(see Fig. 8). Regarding the northern hemisphere of model MR3 at 240 ms, Fig. 5 indicates that θ_2 is often less than -60° , where the magnetic force strongly works. Hence, the magnetic tension is dominant when $-75^\circ \lesssim \theta_1 \lesssim 15^\circ$. If the effect of the toroidal field is taken into account, the upper critical angle become somewhat larger because the toroidal field is considered to be large in the southern hemisphere (see § 3.1). On the other hand, the left-bottom panel of Fig. 8 shows that θ_1 is adequately more than 15° almost everywhere. Therefore the magnetic pressure is dominant there and it becomes a leading force to accelerate the proto-magnetar. The same discussion can be done on the southern hemisphere. In fact in model MR3 (and also in models SR3 and SR10), such a situation is common for almost all time in the computation.

Around 150 – 160 ms in model MR3, the magnetic acceleration decreases, which causes kicking-back of the proto-magnetar northward. This decrease is likely to be yielded by the predominant amplification of the toroidal field in the southern hemisphere around that time (see Fig. 4), which makes the magnetic pressure work northward. After kicking-back, the magnetic stress comes back to life with even greater strength than before. This is because the difference of the magnetic stress between the north and south surfaces becomes larger although the stresses themselves are weaker than before. Then the acceleration gradually decreases as the north-south difference in magnetic stress diminishes. At the end of the computation, the acceleration is quite small, and so the proto-magnetar no longer will be accelerated significantly. Compared with the magnetic stress, the pressure and gravity are less important for the acceleration of the proto-magnetar except for the time of kicking-back. After the northward-shock front passes the north surface of the proto-magnetar in first around 150 ms, the pressure is larger in the vicinity of the north surface. However, this is until the southward shock front passes the south surface of the proto-magnetar with a few ms delay. After this, the pressure in the vicinity of the south surface is always larger because there is more matter or the heat energy. The gravity pulls the proto-magnetar to the direction where there is more matter. However, after 162 ms, a part of matter is ejected out of the numerical domain, but we neglect the gravity from the expelled matter. Hence, the value of the gravitational acceleration in Fig. 7 is not valid after this time. Nevertheless, keeping in mind that the gravitational acceleration is comparable to the acceleration owing

to the pressure, the effect of the gravity on the kick velocity is no significance either way. The same can be said for models SR3 and SR10. For models MS3 and SS3, since the ejected mass is $\sim 0.03M_{\odot}$, the gravitational acceleration changes at most $\sim 10\%$ even if they are taken into account.

In models SR3 and SR10, the time evolution of magnetar velocities and the acceleration mechanisms are similar to that of model MR3. In model SR3, however, the magnetic stress which has accelerated the proto-magnetar southward turns to work oppositely around 210 ms and the proto-magnetar starts to be decelerated. This is probably because the magnetic field becomes locally stronger around the south surface of the proto-magnetar. At the end of the simulation, the magnetic stress still has a positive value. Thus, although the proto-magnetar gets the final velocity of 353 km s^{-1} , this will be decreased later in some degree. Model SR10 produces the highest velocity of proto-magnetar among all models. In spite of the smaller stored magnetic energy than that in model SR3, a considerable north-south difference of them can produce a larger accelerations. In this model, kicking-back occurs due not to reduction of magnetic stress but to the pressure and gravity. At the end of simulation the acceleration is still substantial. It will be negligible around 300 ms if linearly extrapolated. The velocity of the proto-magnetar around that time will be $\sim 1500 - 1600\text{ km s}^{-1}$.

The slow rotation models, MS3 and SS3, show more complex time evolution of the proto-magnetar acceleration (see Fig 7). In each of these cases, the magnetic pressure alone is not always the leading driving force, but the magnetic tension, matter pressure or gravity also play important roles. This is due to a low ratio of the magnetic pressure to matter pressure in the vicinity of the proto-magnetar. Although these models explode weakly, the final magnetar velocity are not differ significantly from those for the more strong explosion models. This is because the kinetic energy of a proto-magnetar whose velocity is \sim a few 100 km s^{-1} is just $\sim 10^{48}$ erg which is even smaller than the explosion energies of model MS3 and SS3. The time evolution of acceleration still varies violently even around the end of the computation. In order to get reliable final velocities, longer numerical simulations are necessary.

3.4.1. *Uncertainties from the definition of A Proto-Magnetar*

As noted in § 2.4, we assume a proto-magnetar as region containing $1.2 M_{\odot}$, which are calculated by summing up the mass of each fluid element in descending order of the density. However, it is admittedly highly uncertain at 240 ms which part of the gas is finally settled to be a proto-magnetar. In fact, this will not be known for sure until computations are done up to the time, by which a fall back of matter has been finished. According to

Zhang et al. (2007), this time is estimated to be about 10^6 s, which is far longer than our computational time, 240 ms, and is, unfortunately, too long to dynamically follow with numerical simulations like ours. What we can do and we should do instead is to make clear the uncertainty of the kick velocities associated with the definition of a proto-magnetar. For this purpose, we have computed another model, which covers a greater portion of the star, and we have also calculated the kick velocities with several alternative definitions of a proto-magnetar, taking model MR3 as an example.

We first investigate the uncertainties coming from the proto-magnetar mass. Five different masses of proto-magnetars, 1.2, 1.23, 1.26, 1.3, 1.35 M_\odot , are tried. We take here the maximal mass to be 1.35 M_\odot anticipating that a proto-magnetar produced by a magnetic prompt explosion will be less massive than 1.4 M_\odot , the canonical value for the ordinary radio pulsars. We then introduce another criterion for a proto-magnetar, by which fluid elements are summed up in the descending order of "pressure" instead of density. Several masses of proto-magnetar are tried again with this "pressure criterion". In the study of proto-magnetars more massive than 1.2 M_\odot , a larger portion of the progenitor star needs to be computed. We thus run another numerical simulation, which computes the evolution of the inner 2.0 M_\odot of the 15 M_\odot progenitor by Woosley (1995) for the same parameter values of $|E_m/W|$, $|T/W|$, and z_{off} as in model MR3, and obtain the kick velocities of 10 different proto-magnetars. We give each model the name as MR3env[D or P] [proto-magnetar's mass], where "D" and "P" denote the density- and pressure-criterion, respectively. For example, a model for 1.23 M_\odot proto-magnetar determined by the pressure-criterion is referred to as MR3envP1.23.

The results are shown in Fig. 9, which illustrates the time evolution of the velocity for each proto-magnetar. We find that the difference in the criterion does not produce a significant variation in the kick velocities. On the other hand, it is found that the difference in the mass of proto-magnetar results in a noticeable variation in the kick velocities. In both series, MR3envD and MR3envP, the velocity tends to decrease with increasing mass. This is because a proto-magnetar with a higher mass has a larger radius and the magnetic field on the surface becomes weaker, which then leads to a smaller north-south difference in the magnetic forces. Note, however, that the most massive proto-magnetar models in our analysis, MR3envD1.35 and MR3envP1.35, still have kick velocities of ~ 200 km s^{-1} .

The kick velocities obtained with several different definitions of a proto-magnetar cover a range of $\sim 200 - 500$ km s^{-1} . We thus consider that the kick velocities we have procure in this study have uncertainty of this degree. We can thus claim that a proto-magnetar is possibly accelerated up to several hundred km s^{-1} by the magnetohydrodynamic process considered in this paper.

4. Discussion and Conclusion

We have done series of numerical simulations of core-collapse supernovae with strong offset-dipole magnetic fields (offset northward) and rapid rotations. Main purposes of our study was investigating how dynamics and magnetar kicks behave with such off-centered magnetic fields. We finally found that:

1. Equatorially-asymmetric explosions occur for all models with a formation of bipolar jets. Jets are fast-light in the north and slow-heavy in the south for the rapid rotation models while they are fast-heavy in the north and slow-light in the south for the slow rotation models.

2. Off-centered magnetic field weaken the explosion for the rapid rotation case. In this case, the explosion energy is larger in the south since less matter is ejected or less magnetic energy is stored in the north. On the other hand, the explosion energy is larger in the north for the slow rotation models.

3. The formed proto-magnetars are slow rotator with the rotational periods of more than 10 ms. The final magnetic field around the proto-magnetar has a collimated dipole-like configuration pinched by the toroidal field lines for the rapid rotation models whereas the proto-magnetar formed in the slow rotation models is totally poloidal-field dominant.

4. If the initial magnetic field is stronger in the northern hemisphere, proto-magnetars are kicked southward with the velocities of several hundred km s^{-1} , or in extreme case $\sim 1000 \text{ km s}^{-1}$. In most cases, they are accelerated mainly by the magnetic pressure while the somewhat weaker magnetic tension works the opposite direction, which is due to stronger magnetic field in the northern hemisphere.

Form the results of computations, we predict that magnetars also possibly have large velocities as ordinary pulsars do and in some extreme cases they could have $\sim 1000 \text{ km s}^{-1}$ velocities. Current observations show that at least some magnetar candidates have the velocities of less than 500 km s^{-1} (see § 1) whereas Duncan & Thompson (1992) claimed that magnetars will have large kick velocities up to $\sim 1000 \text{ km s}^{-1}$. It is notable that our results also show that the some moderate initial conditions lead to the velocities less than $\sim 500 \text{ km s}^{-1}$ which is not inconsistent with the observations. On the other hand, if the association between SGR 0526-66 and N49 or SGR 1627-41 and G337.0-0.1 is true, these magnetar candidates should have an extremely large kick velocities up to $\sim 1000 \text{ km s}^{-1}$. In the context of our numerical simulations, these extraordinarily high velocities are interpreted as the products of the extreme initial condition, i.e. very strong and highly asymmetric magnetic fields as in model SR10.

Some observations of recent date imply that some magnetars are originate from massive

progenitor ($\gtrsim 20 - 50M_{\odot}$) (e.g. Gaensler et al. 2005; Figaer et al. 2005; Muno et al. 2006). We use a $15M_{\odot}$ stellar model although our computation involves a formation of magnetars. This is because a $15M_{\odot}$ star is a canonical progenitor of core-collapse computations and it has not known yet whether a massive-star-origin magnetar is common. However, it is worth investigating in the future whether the similar results to us are yielded by the numerical simulation with more massive progenitors. When the massive progenitors are chosen, it is more natural for us to assume rapid rotation since Heger et al. (2005) argued from their calculation of stellar evolution that more massive stars tend to rotate more rapidly. According to them, $35M_{\odot}$ star will reach the rotation period of the neutron star of 4.4 ms in there standard model, though the magnetic flux of the star is far weaker than that of magnetars and again this result is not conclusive.

The other kick mechanisms introduced in § 1 does not work in the situation considered here. For the hydrodynamically-driven and neutrino-magnetic-field driven mechanism, this is because the kicks are accompanied with delayed explosion while, in our simulation, prompt explosion occurs with the help of strong magnetic field and rotation. In an electromagnetically-driven mechanism, the acceleration time scale is ~ 4 s if the field strength on the surface of the (proto-) magnetar is $\sim 10^{16}$ G, which is much longer than that of “*magnetohydrodynamically-driven kick*”. Our computation shows that the initially rapid rotation becomes quite slow (more than 10 ms rotation period) in $\lesssim 100$ ms after bounce (see § 2.3). Noted that this mechanism requires the rotation period of ~ 1 ms, the proto-magnetar cannot be substantially accelerated.

The above discussion is valid only when the initial conditions which we assume, strong magnetic fields, rapid rotation, and offset dipole fields, are achieved. Although validity of these assumptions is discussed in § 2.3, they are far from solid. What will happen if our assumptions are partially fulfilled? With strong magnetic fields but a slow rotation, the magnetorotational explosion considered here can not occur. In this case, the engine of supernova might be the heating by emitted neutrinos, and the second kick mechanism (neutrino-magnetic field driven) introduced in § 1 might work. We have no idea at the moment whether the hydrodynamical-instability-driven kick (the first mechanism) could operate or not in the presence of strong magnetic fields. This should be investigated in the future works. If the initial magnetic field is weak and rotation is rapid, the magnetorotational explosion may ensue with a help of magnetorotational instability (MRI) or convective dynamo action (e.g. Akiyama et al. 2003; Ardeljan et al. 2005; Duncan & Thompson 1992). However, it needs more detailed studies. Note that in order to reliably compute the growth of MRI from weak magnetic fields of $\sim 10^8 - 10^9$ G in the supernova core, the spatial grid size should be at least as small as $\sim 10^2$ cm, which no numerical simulation has achieved yet so far. Meanwhile, even in the present computations with $\sim 10^{12} - 10^{13}$ G initially, the grid

resolution is not fine enough by a factor of ten in some important regions to resolve MRI. In this case, however, the compression and wrapping-up of the initial field amplify the field strength sufficiently before MRI sets in and we expect MRI will not change the dynamics very much even if it occurs. But, we do not intend to claim that MRI is not important. On the contrary, we are interested in the MRI-related issues such as the linear growth, nonlinear saturation, implications for explosion, pulsar kick and spin and so forth. We think they should be addressed in a separate paper. In so doing, three-dimensional computations are important, which we are now undertaking (Sawai et al. 2008 in preparation).

We find that the centrally concentrated magnetic field has an advantage in energetic explosion. Recently, Pian et al. (2006) reported that SN 2006aj associated with X-ray flash 060218 is a factor 2-3 more luminous than other normal type Ic supernovae although it is dimmer than so-called hypernovae associated with gamma-ray bursts. Mazzali et al. (2006) claimed that the remnant of SN 2006aj is not a black hole but a neutron star, possibly a magnetar. If this is true, a highly energetic explosion induced by centrally-concentrated magnetic fields can be one of the origins of this middle-class supernova although the mechanism to produce the X-ray flash is beyond the scope of this paper. Note that not every supernova accompanied by a magnetar should produce such a energetic explosion. It is reported that for some supernovae, which are considered to be associated with magnetar candidates, the explosion energies are just as large as those of ordinary supernovae (Vink & Kuiper 2005; Sasaki et al. 2004).

Finally, how large a fraction do magnetars occupy among the whole population of isolated neutron stars? At present, the confirmed candidates of magnetars are counted up to eleven which is only $\sim 1\%$ of the observed ordinary pulsars. However it is too early to conclude that magnetars are such a minor population. Spin-down ages are measured in three of four SGRs, which are younger than 1900 years. This means a magnetar is born every ~ 600 years, corresponding to $\sim 15\%$ of ordinary neutron stars. If another magnetar, SGR 1627-41, has a similar spindown age, the number of magnetars are estimated to be $\sim 20\%$ of that of the ordinary pulsars. Here we omit AXPs since there may be a large number of AXPs which are too dim to detect (Woods & Thompson 2006). Woods & Thompson (2006) insisted that there may be a lot of magnetars which are too old to be detected and that the number of magnetars could be comparable to that of ordinary pulsars. If this is the case, the study of the supernova theory in the strong-magnetic-field regime will have a more significant meaning.

H. S. thanks to E. Müller and H.-Th. Janka for useful discussion during his stay at Max-Planck-Institute für Astrophysik. H. S. also thanks D. Lai for helpful discussion. Some of the numerical simulations were done on the supercomputer VPP700E/128 at RIKEN and

VPP500/80 at KEK (KEK Supercomputer Projects No. 108). This work was partially supported by the Japan Society for Promotion of Science (JSPS) Research Fellowships (H.S.), the Grants-in-Aid for the Scientific Research (14079202, 17540267) from Ministry of Education, Science and Culture of Japan, and by the Grants-in-Aid for the 21th century COE program “Holistic Research and Education Center for Physics of Self-organizing Systems”.

REFERENCES

- Akiyama, S., Wheeler, J. C., Meier, D. L., & Lichtenstadt, I. 2003, *ApJ*, 584, 954
- Ardeljan, N. V., Bisnovatyi-Kogan, G. S., & Moiseenko S. G. 2005, *Mon. Not. R. Astron. Soc.*, 359, 333
- Arras, Ph. & Lai, D. 1999, *Phys. Rev. D*, 60, 043001
- Bisnovatyi-Kogan, G. S., Popov, YU. P., & Samochin, A. A. 1975, *Ap&SS*, 41, 287B
- Braithwaite, J., & Spruit H. C., 2004, *Nature*, 431, 819
- Cline, T. L. et al. 1982, *ApJ*, 255, L45
- Corbel, S., Chapuis, C., Dame, T. M., & Durouchoux, P. 1999, *ApJ*, 526, L29
- Cordes, J. M., & Chernoff, D. F. 1998, *ApJ*, 505, 315
- Donati, J.-F., Babel, J., Harries, T. J., Howarth, I. D., Petit, P., & Semel, M. 2002, *Mon. Not. R. Astron. Soc.*, 333, 55
- Donati, J.-F., Howarth, I. D., Bouret, J.-C., Petit, P., Catala, C., & Landstreet, J. 2006, *Mon. Not. R. Astron. Soc.*, 365, L6
- Duncan, R. C., & Thompson, C. 1992, *ApJ*, 392, L9
- Ferrario, L. & Wickramasinghe, D. T. 2005, *Mon. Not. Astron. Soc.*, 356, 615
- Figer, D. F., Najarro, F., Geballe, T. R., Blum, R. D., & Kudritzki, R. P. 2005, *ApJ*, 622, L49
- Fryer, C. L., & Warren, M. S. 2004, *ApJ*, 601, 391
- Gaensler, B. M., McClure-Griffiths, N. M., Oey, M. S., Haverkorn, M., Dickey, J. M., & Green, A. J. 2005, *ApJ*, 620, L95

- Gaensler, B. M., Slane, P. O., Gotthelf, E. V., & Vasisht, G. 2001, *ApJ*, 559, 963
- Gunn, J. E., & Ostriker, J. P. 1979, *ApJ*, 160, 979
- Goldreich, P. & Reisenegger, A. 1992, *ApJ*, 395, 250
- Harrison, E. R. & Tademaru, E. 1975, *ApJ*, 201, 447
- Heger, A., Woosley, S. E., & Spruit, H. C. 2005, *ApJ*, 626, 350
- Hobbs, G., Lorimer, D. R., Lyne, A. G., & Kramer, M. 2005, *Mon. Not. R. Astron. Soc.*, 360, 974
- Hubrig, S., Briquet, M., Schöller, M., De Cat, P., Mathys, G., & Aerts, C. 2006, *Mon. Not. Astron. Soc.* 369, L61
- Hulleman, F., van Kerkwijk, M. H., & Kulkarni, R. 2000, *Nature*, 408, 689
- Kotake, K., Sawai, H., Yamada, S., & Sato, K. 2004, *ApJ*, 608, 391
- Kotake, Yamada, S., & Sato, K. 2005, *ApJ*, 618, 474
- Lai, D. 2003, *Proc. “Cosmic explosions in three dimensions: asymmetries in supernovae and gamma-ray bursts”*, p276
- Lai, D. & Qian, Y. 1998, *ApJ*, 505, 844
- LeBlanc, J. M., & Wilson, J. R. 1970, *ApJ*, 161, 541
- Mazzali, P. A. et al. 2006, *Nature*, 442, 1018
- Moiseenko, S. G., Bisnovatyi-Kogan, G. S., & Ardeljan, N. V. 2006, *Mon. Not. R. Astron. Soc.*, 310, 501
- Müller, E., & Hillebrandt, W. 1979, *Astron. Astrophys.*, 80, 147
- Muno, M. P. et al. 2006, *ApJ*, 636, L41
- Neiner, C., Geers, V. C., Henrichs, H. F., Floquet, M., Frémat, Y., Hubert, A. -M., Preuss, O., & Wiersema, K. 2003a, *A&A*, 406, 1019
- Neiner, C., Hubert, A. -M., Frémat, Y., Floquet, M., Jankov, S., Preuss, O., Henrichs, H. F., & Zorec, J. 2003b, *A&A*, 409, 275
- Neiner, C., Henrichs, H. F., Floquet, M., Frémat, Y., Preuss, O., Hubert, A. -M., Geers, V. C., Tijani, A. H., Nichols, J. S., & Jankov, S. 2003c, *A&A*, 411, 565

- Nishimura, S., Kotake, K., Hashimoto, M., Yamada, S., Nishimura, N., Fujimoto, S., & Sato, K. 2006, *ApJ*, 642, 410
- Obergaulinger, M., Aloy, M. A., & Müller, E. 2006, *A&A*, 450, 1107
- Ögelman, H. & Tepedelenlioğlu 2005, astro-ph/0503215, submitted to *ApJ*
- Ohnishi, T. 1983, Tech. Rep. Inst. At. En. Kyoto Univ. No.198
- Paczyński, B. 1992, *Acta Astronomica*, 42, 145
- Pian, E. et al. 2006, *Nature*, 442, 1101
- Sasaki, M., Plucinsky, P. P., Gaetz, T. J., Smith, R. K., Edgar, R. J., & Slane, P. O. 2004, *ApJ*, 617, 322
- Sawai, H., Kotake, K. & Yamada, S. 2005, *ApJ*, 631, 446
- Scheck, L., Kifonidis, K., Janka, H.-Th., & Müller, E. 2006, *A&A*, 457, 963
- Shibata, M., Liu, Y. T., Shapiro, S. L., & Stephens, B. C. 2006, accepted for publication in *Phys. Rev. D*, astro-ph/0610840
- Stone, J. M., & Norman M. L. 1992, *ApJS*, 80, 791
- Symbalisty, E. M. D. 1984, *ApJ*, 285, 729
- Takahara, M. & Sato, K. 1984, *Prog. Theor. Phys.*, 71, 524
- Takiwaki, T., Kotake, K., Nagataki, S., & Sato, K. 2004, *ApJ*, 616, 1086
- Taylor, J. H. & Weisberg, J. M. 1982, *ApJ*, 253, 908
- Thompson, C., & Duncan, R. C. 1992, *ApJ*, 408, 194
- Thompson, C., & Duncan, R. C. 1995, *Mon. Not. R. Astron. Soc.*, 275, 255
- Thompson, C., & Duncan, R. C. 1996, *ApJ*, 473, 322
- Thorsett, S. E. & Chakrabarty, D. 1999, *ApJ*, 512, 288
- Vink, J. & Kuiper, L. 2005, *Mon. Not. R. Astron. Soc.*, 370, L14
- Wheeler, J. C., Meier, D. L., & Wilson, J. R. 2002, *ApJ*, 568, 807
- Wickramasinghe, D. T. & Ferrario, L. 2005, *Mon. Not. Astron. Soc.*, 356, 1576

Woods, P. M. & Thompson, C. 2006, *Compact Stellar X-ray Sources* (Cambridge Astrophysics Series), 547

Woosley, S. E. 1995, private communication

Yamada, S., & Sato, K. 1994, *ApJ*, 434, 268

Yamada, S., & Sawai, H. 2004, *ApJ*, 608, 907

Zhang, W., Woosley, S. E., & Heger, A. 2007, submitted to *ApJ*, astro-ph/0701083

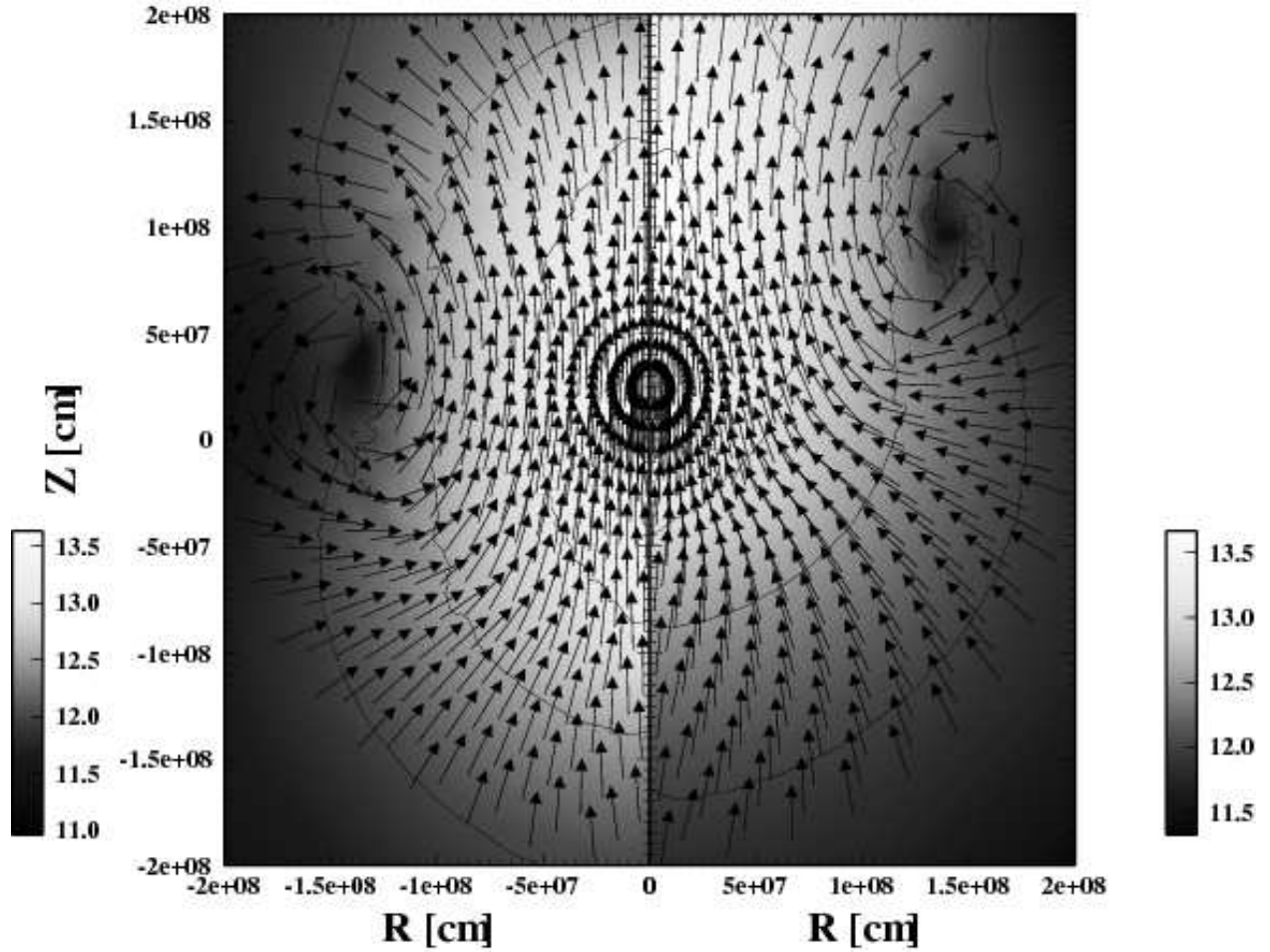


Fig. 1.— The initial magnetic magnetic fields of models MR3 (left panel) and SR10 (right panel). Gray colors show the strengths of the poloidal magnetic fields and the vectors represent the directions of the magnetic fields. The initial radius of the $1.5 M_{\odot}$ core is 2000 km.

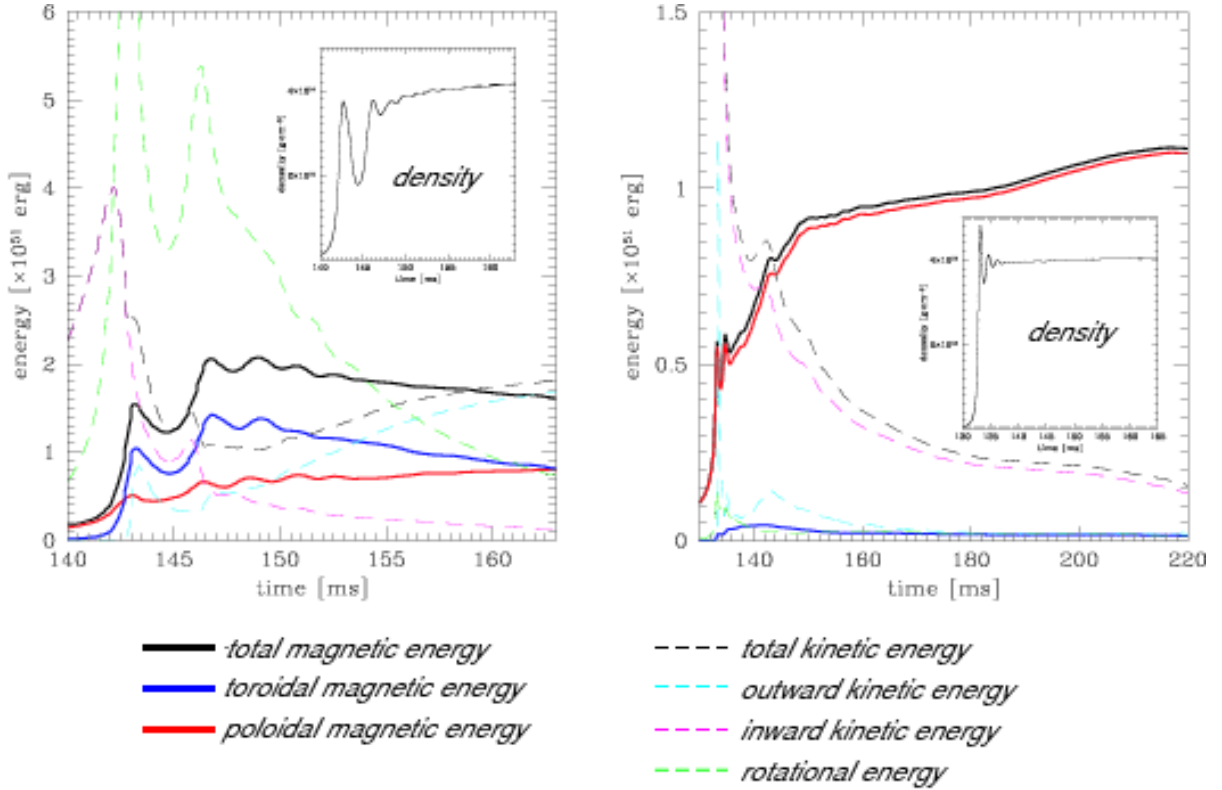


Fig. 2.— The time evolutions of the rotational, kinetic, poloidal magnetic, and toroidal magnetic energy until the farthest shock reaches a radius 1500 km. the left and right panels correspond to model MR0 and MS3, respectively. “Outward kinetic energy” and “inward kinetic energy” are defined as the kinetic energy of matters whose radial velocity is positive and negative, respectively.

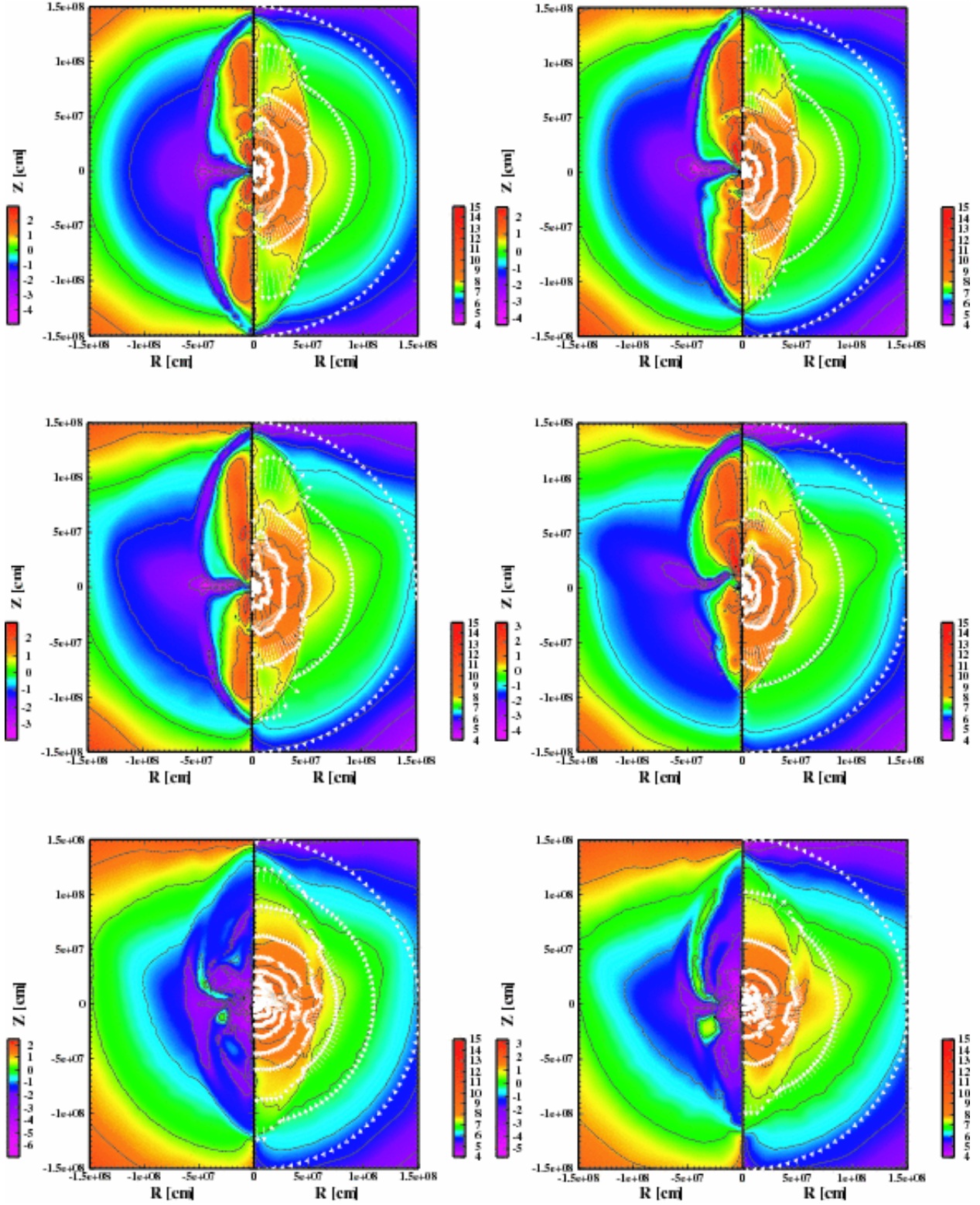


Fig. 3.— The velocity fields on top of the density color contours (the right half of each panel), and the contours of the ratio of the magnetic pressure to matter pressure (the left half of each panel) when the shock front reaches a radius of about 1500 km. From left to right and top to bottom, panels of model MR0, MR3, SR3, SR10, MS3, and SS3 are displayed in sequence. In each panel, colors in the region out of a radius of 1500 km are extrapolated.

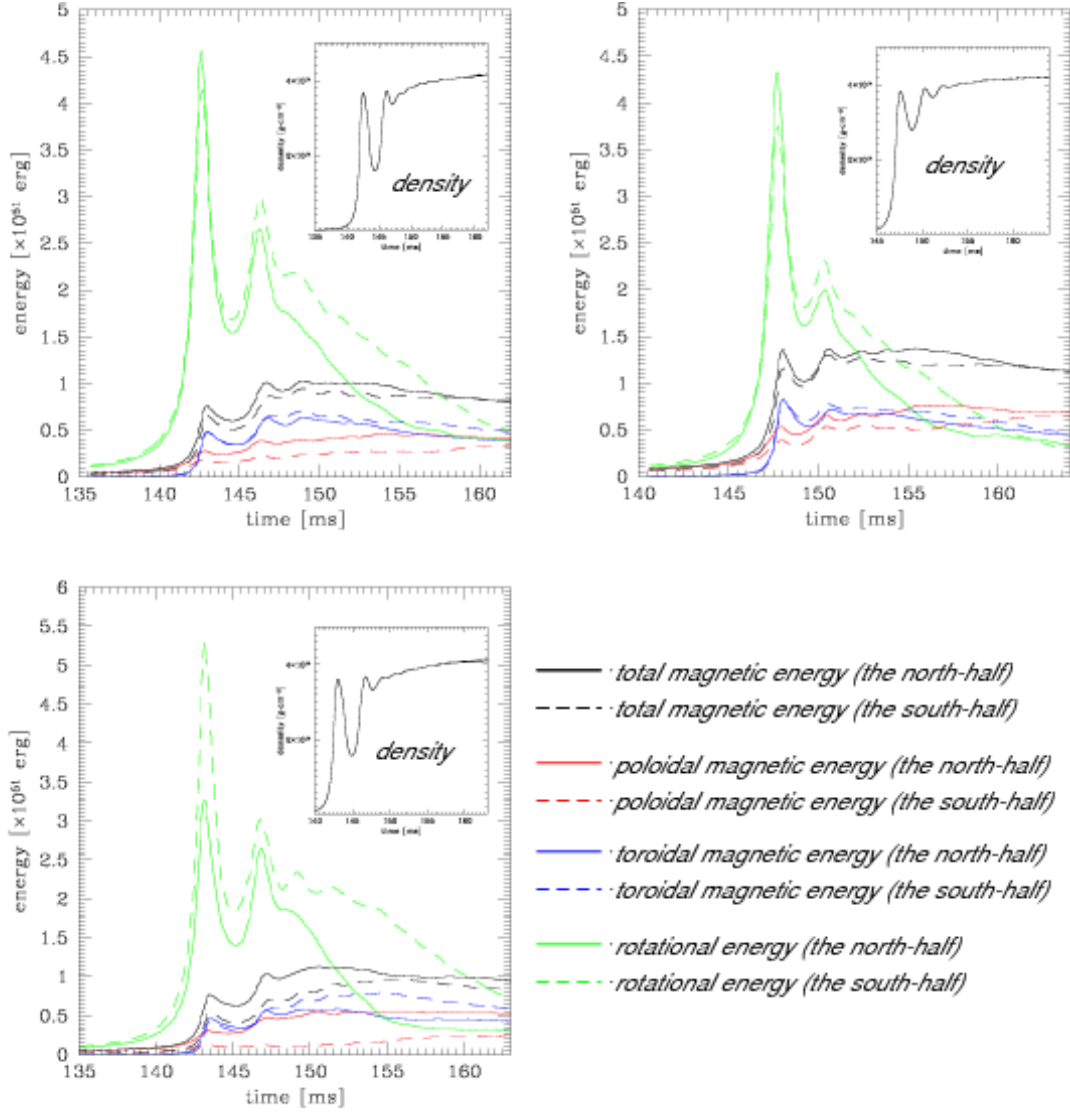


Fig. 4.— The time evolution of the total, poloidal, and toroidal magnetic energy and the rotational energy. The energies of the northern and southern hemisphere are drawn separately. The insets show the time evolution of the central density. Figures of models MR3, SR3, and SR10 are put in order from left to right and top to bottom.

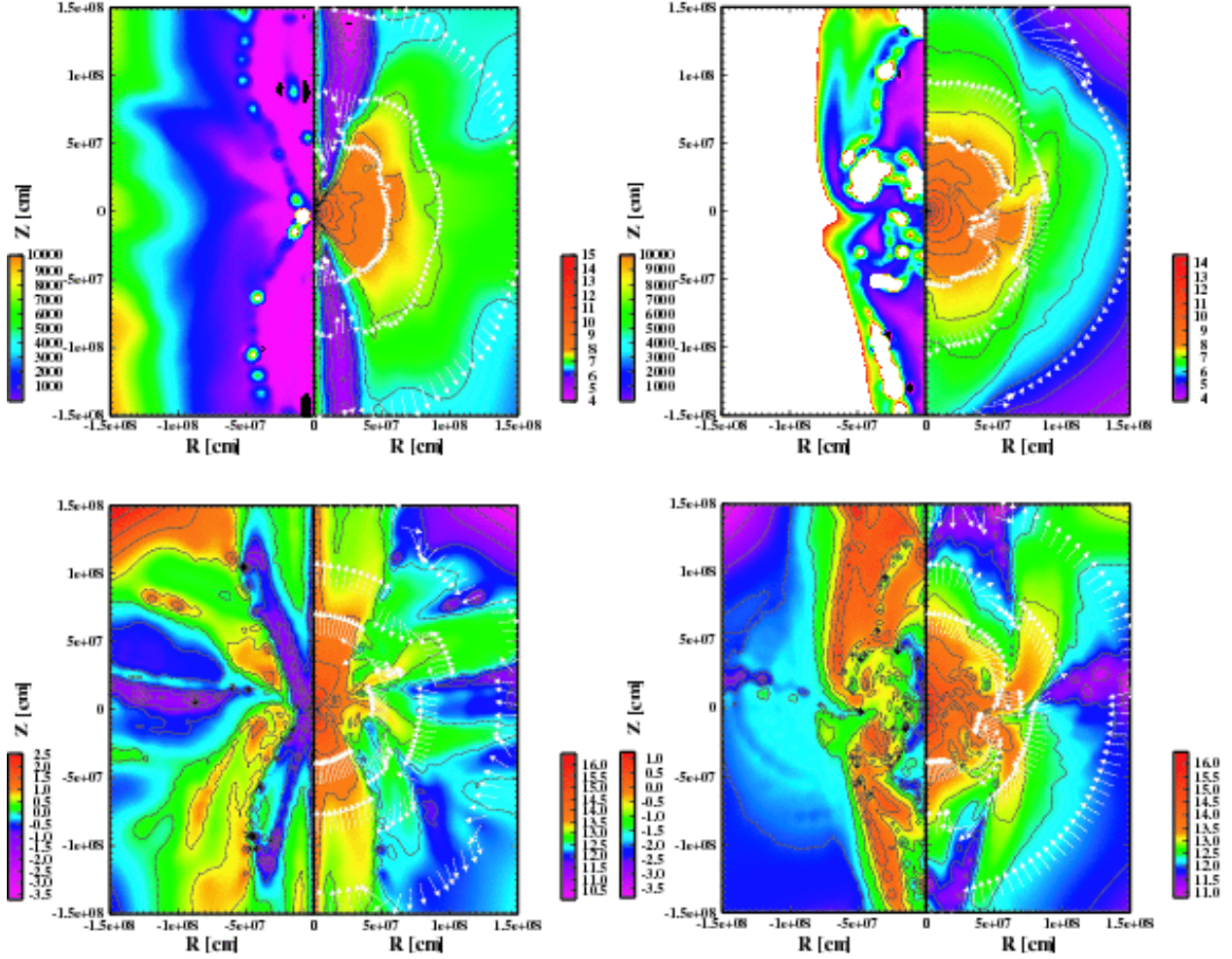


Fig. 5.— Upper two panels: The density contours (the right half of each panel), and the contours of the rotation period in millisecond (the left half of each panel) at 240 ms from the beginning for models MR3 (the left panel) and MS3 (the right panel). In the left half of each panel, the white-colored and black-colored regions have rotation period of more than 10 s and less than 10 ms, respectively. The vectors in the right-half of each panel represent the velocity field. Lower two panels: The contours of the poloidal field strength (the right half of each panel), and the contours for the ratio of the toroidal to poloidal field strength (the left half of each panel) at 240 ms from the beginning for models MR3 (the left panel) and MS3 (the right panel). The vectors in the right-half of each panel represent the directions of the poloidal magnetic field.

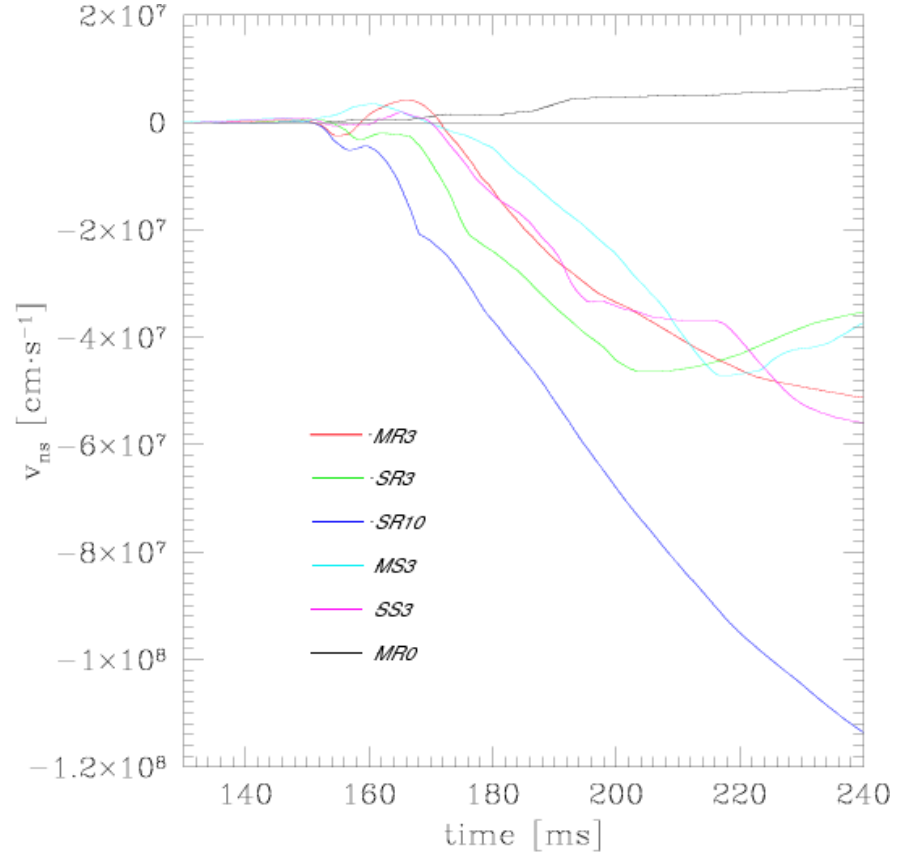


Fig. 6.— Time evolutions of the proto-magnetar velocities. The northward velocity is taken to be positive.

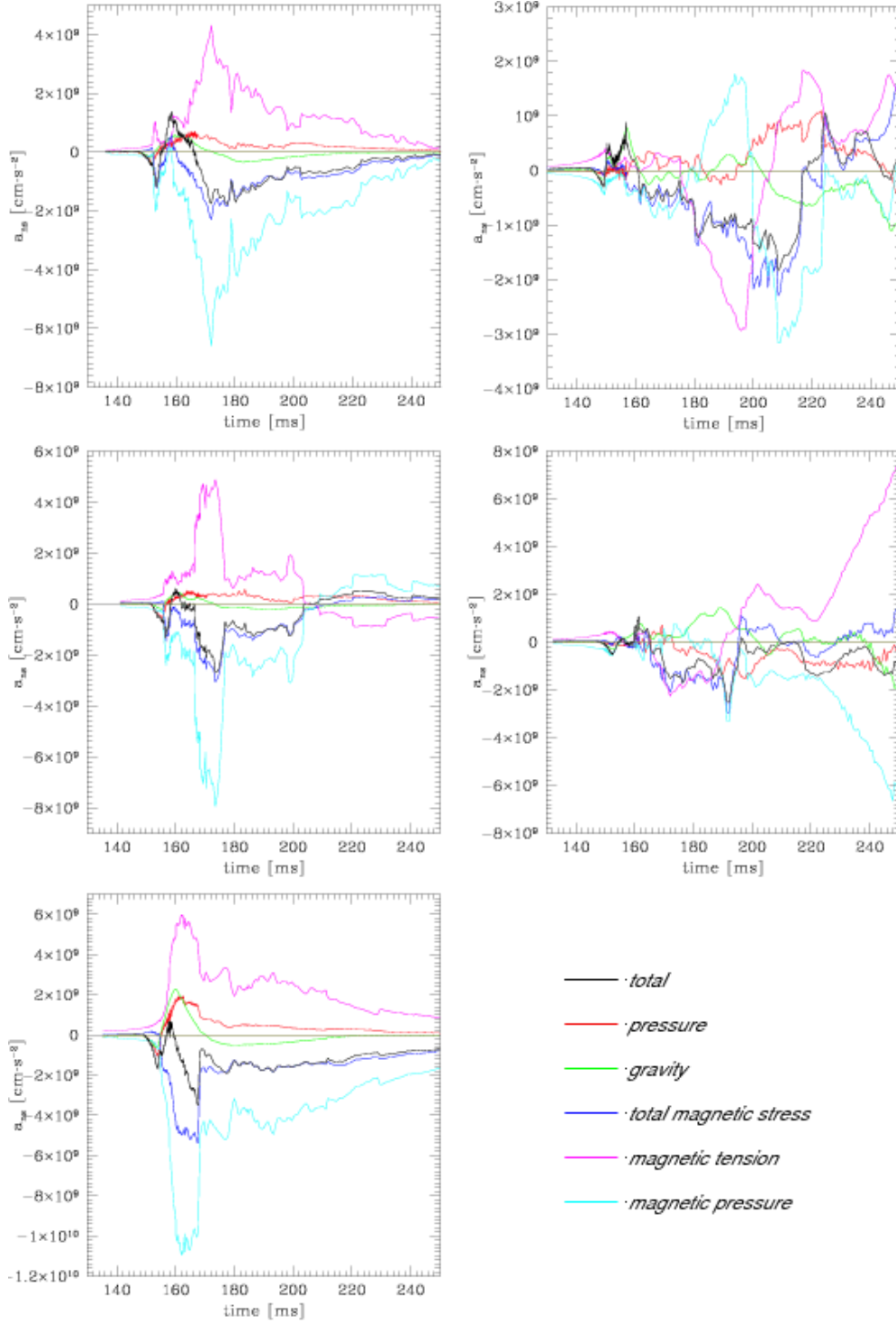


Fig. 7.— Time evolutions of the accelerations acting on the proto-magnetar star. The magnetic acceleration divided into two parts, the tension part and pressure part. From top to bottom and left to right, panels of model MR3, SR3, SR10, MS3, and SS3 are displayed in sequence. The northward acceleration is taken to be positive.

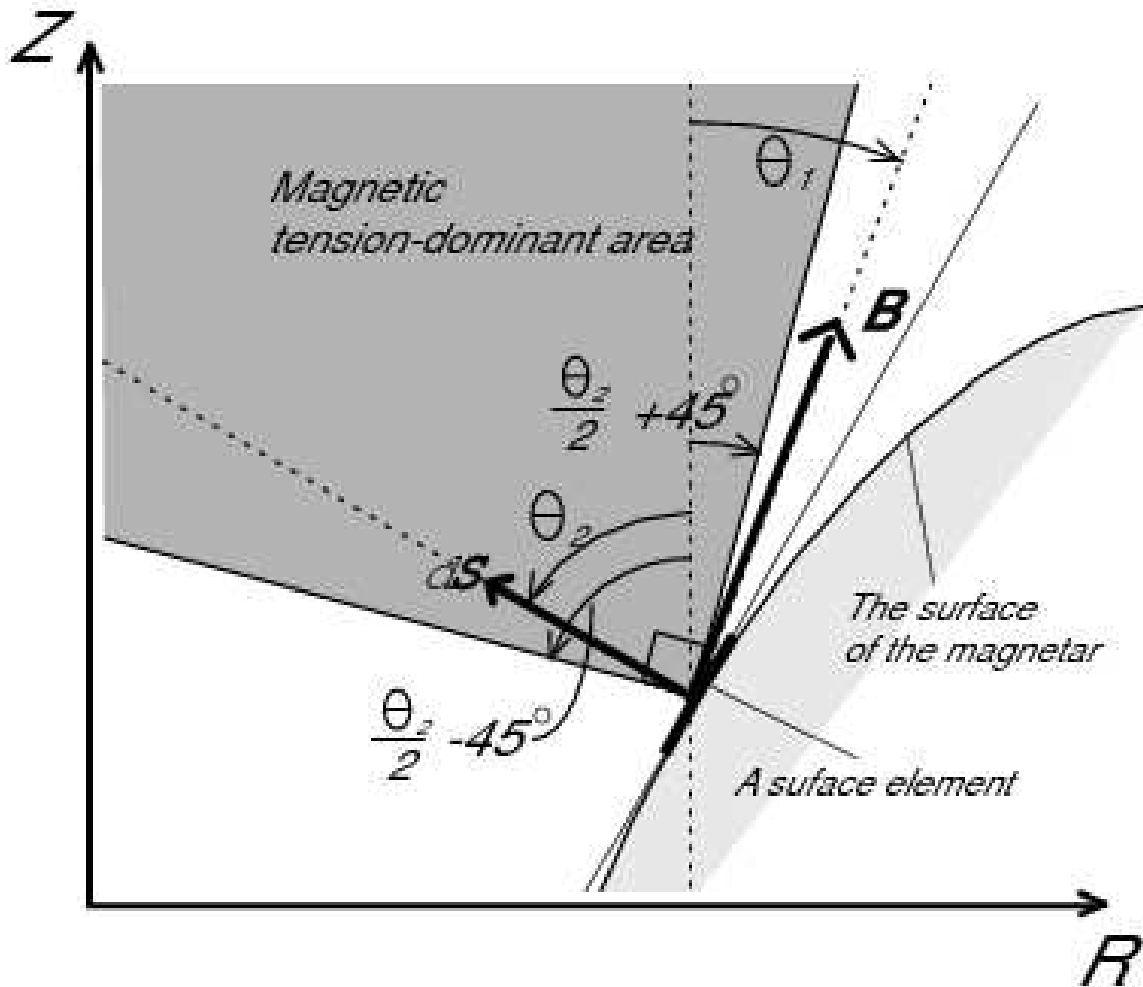


Fig. 8.— A schematic picture which shows the magnetic tension-dominant area (strong gray colored). \mathbf{B} and $d\mathbf{S}$ is the magnetic field vector and surface vector, respectively. θ_1 and θ_2 are the angles from the rotation axis to the magnetic field vector and surface vector, respectively, taking clockwise rotation positive.

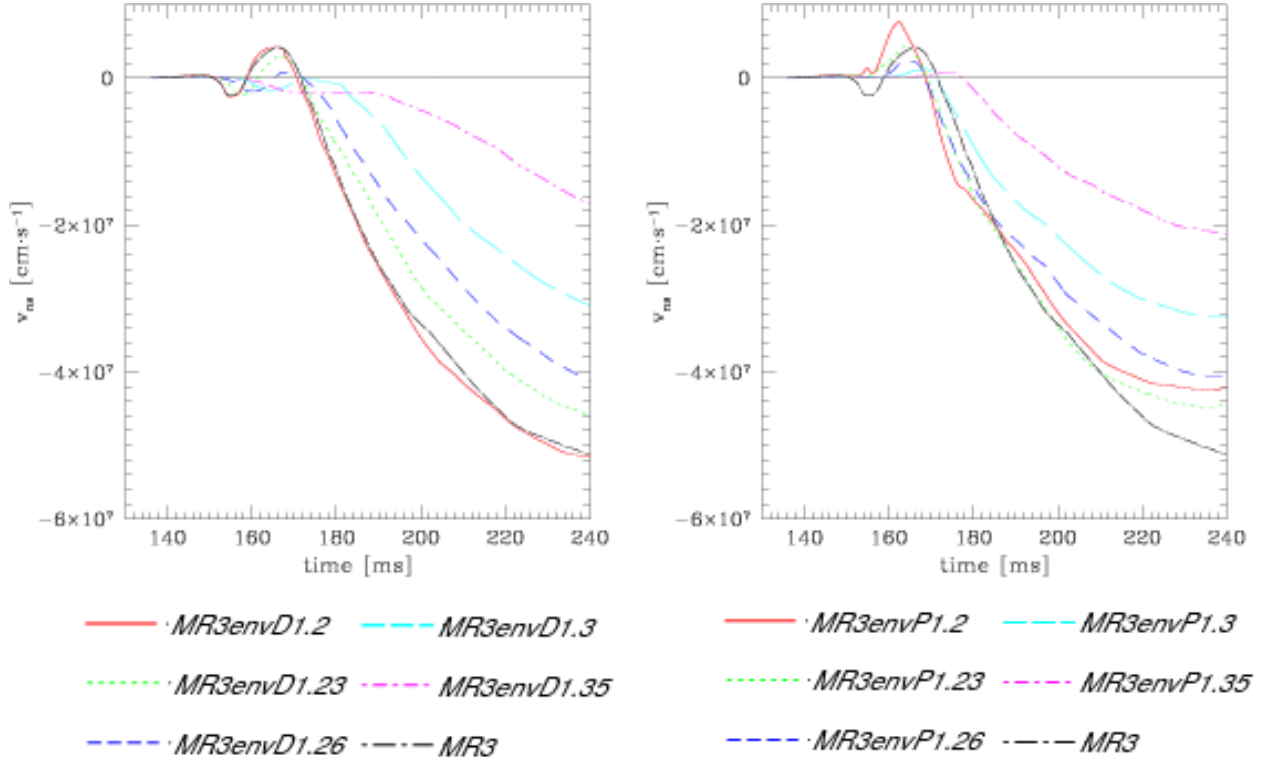


Fig. 9.— Time evolutions of the proto-magnetar velocities for several definitions of a proto-magnetar. Left and right panel corresponds to the results of model series of MR3envD and MR3envP, respectively. In each panel, solid, dotted, short-dashed, long-dashed, and dotted-short-dashed, lines correspond to model of 1.2, 1.23, 1.26, 1.3, and 1.35 M_{\odot} proto-magnetars, whereas dotted-long-dashed line is drawn for model MR3 for comparison. The northward velocity is taken to be positive.

Table 1: **Initial Parameters**

Model	$ E_m/W $ [%]	$ T/W $ [%]	B_i [G]	Ω_i [rad s ⁻¹]	z_{off} [km]
MR0	0.5	0.5	5.6×10^{13}	3.9×10^0	0
MR3	0.5	0.5	4.6×10^{13}	3.9×10^0	300
MS3	0.5	0.005	4.6×10^{13}	3.9×10^{-1}	300
SR3	1.0	0.5	6.5×10^{13}	3.9×10^0	300
SR10	1.0	0.5	4.9×10^{13}	3.9×10^0	1000
SS3	1.0	0.005	6.5×10^{13}	3.9×10^{-1}	300

Note. — $|E_m/W|$: the magnetic energy normalized by the gravitational energy. $|T/W|$: the rotation energy normalized by the gravitational energy. B_i : the initial maximum magnetic field. Ω_i : the initial angular velocity at the center of the core. z_{off} : the degree of magnetic-field displacement (see Eq. 8- 9).

Table 2. Key Parameters

Model	$ E_m/W _b$	$ T/W _b$	$B_{b,max}$	$\Omega_{b,max}$	$ E_m/W _{t_1}$	$ T/W _{t_1}$	$B_{t_1,max}$	$\Omega_{t_1,max}$	$r_{sh,u}/r_{sh,d}$	v_{NS}
MR0	1.5	8.0	5.3×10^{16}	6.5×10^4	1.6	0.71	6.3×10^{16}	1.6×10^4	0.97	65
MR3	1.4	8.2	8.3×10^{16}	7.3×10^4	1.6	0.87	6.2×10^{16}	1.9×10^4	1.15	512
MS3	0.50	0.13	1.2×10^{17}	5.8×10^3	0.98	0.016	3.1×10^{16}	1.6×10^2	1.20	374
SR3	1.6	7.5	1.1×10^{17}	6.0×10^4	2.1	0.59	8.1×10^{16}	2.6×10^4	1.17	353
SR10	0.76	7.8	9.0×10^{16}	7.9×10^4	1.6	1.1	4.8×10^{16}	1.4×10^4	1.51	1136
SS3	0.94	0.089	1.3×10^{17}	2.1×10^4	1.5	0.021	4.7×10^{16}	3.6×10^4	1.21	560

Note. — The ratios $|E_m/W|$ and $|T/W|$ are given in percentage. B_{max} : the maximum magnetic field in G. Ω_{max} : the maximum angular velocity in rad s^{-1} . $r_{sh,u}/r_{sh,d}$: the ratio north-shock radius to south-shock radius. v_{NS} : the velocity of the magnetar in km s^{-1} at 240 ms from the beginning. For each parameter, the subscripts “b” and “ t_1 ” denote the values at bounce and those when the shock front reaches radius of 1500 km, respectively.

Table 3: Ejected Mass and Explosion Energy

Model	$M_{ej,tot}$	$M_{ej,n}$	$M_{ej,s}$	$E_{exp,tot}$	$E_{exp,n}$	$E_{exp,s}$
MR0	0.31	0.15	0.15	4.4	2.2	2.2
MR3	0.28	0.11	0.16	4.1	1.8	2.3
MS3	0.029	0.017	0.012	0.38	0.20	0.17
SR3	0.25	0.11	0.15	4.6	2.1	2.5
SR10	0.27	0.095	0.17	4.0	1.8	2.4
SS3	0.036	0.021	0.015	0.56	0.33	0.23

Note. — M_{ej} : the ejected mass in M_{\odot} . E_{exp} : the explosion energy in 10^{51} erg. Subscripts “n”, “s”, and “tot” denote the values in the northern hemisphere, the southern hemisphere, and total values, respectively.